

Non-synchronous strain effects on a hetero-bonded van der Waals material CrSBr

Junming Guo(郭俊明), Wenqiang Shi(时文强), Kaipeng Ni(倪凯鹏), Xing Chen(陈行), Daxiang Liu(刘大象), Xue Liu(刘学), Shouguo Wang(王守国), Qian Li(李倩), Rui-Chun Xiao(肖瑞春), and Mengmeng Yang(杨蒙蒙)
Citation: Chin. Phys. B, 2025, 34 (**10**): 104203. DOI: 10.1088/1674-1056/add90d
http://cpb.iphy.ac.cn; http://iopscience.iop.org/cpb

What follows is a list of articles you may be interested in

Optical trapping capability of tornado circular Pearcey beams

Na-Na Liu(刘娜娜), Xiao-Ying Tang(唐晓莹), Shun-Yu Liu(刘舜禹), and Yi Liang(梁毅)
Chin. Phys. B, 2024, 33 (**5**): 054201. DOI: 10.1088/1674-1056/ad3347

Effectively modulating spatial vortex four-wave mixing in a diamond atomic system

Nuo Ba(巴诺), Ming-Qi Jiang(姜明奇), Jin-You Fei(费金友), Dan Wang(王丹), Hai-Lin Jiang(蒋海林), Lei Wang(王磊), and Hai-Hua Wang(王海华)
Chin. Phys. B, 2024, 33 (**4**): 044202. DOI: 10.1088/1674-1056/ad0771

Temperature-free mass tracking of a levitated nanoparticle

Yuan Tian(田原), Yu Zheng(郑瑜), Lyu-Hang Liu(刘吕航), Guang-Can Guo(郭光灿), and Fang-Wen Sun(孙方稳)
Chin. Phys. B, 2023, 32 (**7**): 074207. DOI: 10.1088/1674-1056/accb4c

Optical pulling force on nanoparticle clusters with gain due to Fano-like resonance

Jiangnan Ma(马江南), Feng Lv(冯侣), Guofu Wang(王国富), Zhifang Lin(林志方), Hongxia Zheng(郑红霞), and Huajin Chen(陈华金)
Chin. Phys. B, 2023, 32 (**1**): 014205. DOI: 10.1088/1674-1056/ac9de5

Graphene-tuned threshold gain to achieve optical pulling force on microparticle

Hong-Li Chen(陈鸿莉) and Yang Huang(黄杨)
Chin. Phys. B, 2021, 30 (**6**): 064205. DOI: 10.1088/1674-1056/abd9b4

Non-synchronous strain effects on a hetero-bonded van der Waals material CrSBr

Junming Guo(郭俊明)[1,†], Wenqiang Shi(时文强)[1,†], Kaipeng Ni(倪凯鹏)[1], Xing Chen(陈行)[1], Daxiang Liu(刘大象)[2], Xue Liu(刘学)[1], Shouguo Wang(王守国)[1], Qian Li(李倩)[2,‡], Rui-Chun Xiao(肖瑞春)[1,§], and Mengmeng Yang(杨蒙蒙)[1,¶]

[1] *Anhui Provincial Key Laboratory of Magnetic Functional Materials and Devices, Faculty of Materials Science and Engineering, Anhui University, Hefei* 230601, *China*
[2] *National Synchrotron Radiation Laboratory, School of Nuclear Science and Technology, University of Science and Technology of China, Hefei* 230029, *China*

(Received 21 April 2025; revised manuscript received 13 May 2025; accepted manuscript online 15 May 2025)

The van der Waals (vdW) material CrSBr exhibits a distinctive hetero-bonded structure, characterized by fence-like and rectangular configurations viewed from different crystallographic orientations. Mechanical deformation of this unique structure can induce significant anisotropic electronic and optical properties. In this study, we systematically investigate the non-synchronous strain response of CrSBr through theoretical and experimental approaches. Our results reveal that the electronic band structure of CrSBr is predominantly governed by the intralayer Cr–S bonds along the *b*-axis, whereas the characteristic Raman peak A_g^3 arises from interlayer Cr–S bond vibrations in each quasi-monolayer. Notably, the different strain responses of these two types of bonds, stemming from the hetero-bonded architecture, lead to distinct behaviors in photoluminescence (PL) and Raman spectra under uniaxial strain. Specifically, the electronic band structure demonstrates heightened sensitivity to tensile strain along the *b*-axis, while the A_g^3 Raman mode exhibits greater sensitivity to strain along the *a*-axis. These insights advance the understanding of strain-induced anisotropies in CrSBr and provide valuable guidance for the design of vdW-based optoelectronic devices.

Keywords: hetero-bond, uniaxial strain, CrSBr

PACS: 42.50.Wk, 68.65.–k, 78.67.–n

DOI: 10.1088/1674-1056/add90d **CSTR:** 32038.14.CPB.add90d

Two-dimensional (2D) van der Waals (vdW) materials represent a distinct class of layered crystals, exemplified by graphite,[1,2] black phosphorus (BP),[2–6] transition metal dichalcogenides (TMDs) MX_2 (M = Mo, W; X = S, Se),[2,7,8] and transition metal phosphorus chalcogenides MPX_3 (M = Mn, Fe, Co, Ni; X = S, Se).[9] These materials demonstrate exceptional mechanical exfoliation capabilities down to monolayer thickness, establishing them as pivotal platforms for fundamental investigations and technological applications in 2D electronics and optoelectronics. While prototypical vdW systems such as graphene and hexagonal boron nitride (h-BN) maintain absolute atomic monolayer configurations, the majority exhibit vertically stacked multiple sublayers interconnected through covalent bonding within quasi-monolayer architectures, which manifests as a fence-like arrangement from side view illustrated in Fig. 1(a). When tensile strain was applied to this kind of fence-like structures, the chemical bond usually elongated isotropically, which leads to isotropic electrical or optical responses. This behavior is exemplified by MoS_2 monolayers, where in-plane tensile strain induces uniform extension of Mo–S covalent bonds.[2,7,8] Similar strain response have also been experimentally verified in ReX_2 (X = S, Se) systems, where the Raman and photoluminescence spectra display the same monotonic trend under the applied strain along *b* axis.[10,11]

In contrast to the most popular fence-like structure, there is rarely alternative rectangular lattice configurations within quasi-monolayer structure, as shown in Fig. 1(b). Uniaxial tensile strain induces bond elongation along the strained axis while simultaneously provoking compressive lattice distortion in orthogonal crystallographic directions. Notably, such rectangular architectures remain exceptionally rare among vdW materials, with black phosphorus representing the sole reported exception exhibiting this structural coupled with anomalous negative Poisson's ratio.[3] This structural dichotomy between fence-like and rectangular vdW configurations raises a fundamental question regarding strain-mediated electronic and optical response: What distinct response mechanisms emerge when comparing conventional fence-like configurations with rectangular lattice systems in vdW materials,

[†]These authors contributed equally to this work.
[‡]Corresponding author. E-mail: liqian89@ustc.edu.cn
[§]Corresponding author. E-mail: xiaoruichun@ahu.edu.cn
[¶]Corresponding author. E-mail: mmyangphy@ahu.edu.cn

© 2025 Chinese Physical Society and IOP Publishing Ltd. All rights, including for text and data mining, AI training, and similar technologies, are reserved.

and how do their respective bonding topologies govern these phenomena? The A-type vdW semiconductor CrSBr presents an ideal platform for such investigations due to its unique hetero-bonded structure.

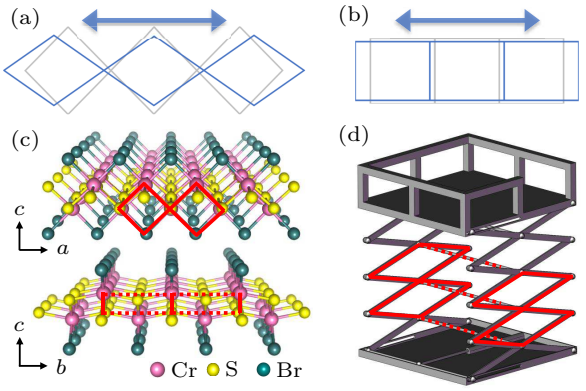


Fig. 1. Schematic illustrations of (a) fence-like and (b) rectangular-like (side view) vdW materials under uniaxial tensile strain. (c) The crystal structure of vdW CrSBr. (d) Schematic diagram of a scissor lift. The red diamond and dashed rectangular represents the fence-like and rectangular-like structures in CrSBr crystal structure.

In recent years, the A-type antiferromagnetic vdW semiconductor CrSBr has garnered significant attention owing to its high air stability, relatively high Néel temperature, and pronounced in-plane magnetic,[12–19] electronic,[20–22] and optical[16,17,22] anisotropies, making it a promising candidate for optoelectronic devices. The crystal structure of CrSBr (Fig. 1(c)) forms both fence-like atomic bonds structure at *ac* plane and rectangular-like structure at *bc* plane, leading to the hetero-bonded structure. This unique architecture, reminiscent of a scissor lift (see Fig. 1(d)), implies that the material may exhibit markedly different mechanical responses when uniaxial tensile strain is applied along the in-plane *a*- and *b*-axes. Consequently, as a hetero-bonded vdW material embodying both fence-like and rectangular-like structures within each quasi-monolayer, CrSBr is expected to respond to strain in a manner distinct from other vdW materials. Notably, a recent study has demonstrated a reversible strain-induced magnetic phase transition in CrSBr when uniaxial tensile strain is applied along the *a*-axis, with the Raman-active A_g^3 mode undergoing a significant shift while the bandgap remains largely insensitive to the strain.[17] Considering the unique crystalline anisotropy, it is essential to apply strain along distinct crystallographic directions to fully elucidate the strain-dependent phenomena, thereby comprehensive theoretical and experimental investigations involving simultaneous uniaxial strain along both in-plane directions are quite necessary.

In this work, we apply uniaxial tensile strain simultaneously along both in-plane *a*- and *b*-axes of CrSBr to examine the anisotropic responses in electronic structure and phonon vibration modes via photoluminescence (PL) and Raman spectra, respectively. Complementary first-principles calculations were employed to investigate the evolution of bandgap, phonon and atomic bond lengths under strain. Our findings reveal that the PL and Raman spectral features exhibit non-synchronous modifications with respect to the direction of the applied strain, indicating a distinct response between the intralayer Cr–S bonds and the interlayer Cr–S bonds within each quasi-monolayer.

CrSBr bulk crystals were grown by chemical vapor transport.[23] The CrSBr flakes were mechanically exfoliated on SiO_2/Si substrates and thickness was verified by atomic force microscopy (AFM). Then an efficient strain engineering approach by encapsulating CrSBr flakes in a flexible polyvinyl alcohol (PVA)[8,24,25] was used (Note S1, supplementary material) to apply uniaxial tensile strain simultaneously along both the *a*- and *b*-axes. Raman and PL measurements were conducted using a micro-Raman spectrometer (LabRAM Horiba Odyssey, Fig. S1, supplementary material) with a $\times 100$ objective lens (NA = 0.90). The first-principles calculations based on DFT are performed using VASP software.[26,27]

We first performed PL and Raman spectra measurements on unstrained CrSBr crystals (Fig. S1, supplementary material). Thickness-dependent measurements revealed negligible variations in peak positions (Fig. S2, supplementary material). As illustrated in Fig. 2(a), the PL peak of CrSBr is located at approximately 1.31 eV, in agreement with previous reports.[17,22,28] Notably, the intensity of PL peaks measured along the *b*-axis (90°) is considerably higher than that along the *a*-axis (0°), with an anisotropy ratio of approximately 3.5. Consequently, polarization-dependent PL measurements were conducted to further elucidate the anisotropic optical behavior of CrSBr. The inset of Fig. 2(a) clearly demonstrates a two-fold anisotropy in the PL peak intensity. To clarify the origin of this anisotropy, we calculated the electronic structure of CrSBr using density functional theory (Note S4, supplementary material). Our calculations indicate that the wavefunctions near both the valence band maximum (VBM) and conduction band minimum (CBM) are predominantly composed of bonding and antibonding states associated with intralayer Cr–S bonds within the quasi-layer oriented along the *b*-axis (inset of Fig. 2(b)). This quasi-one-dimensional character of the band-edge electronic structure subsequently leads to optical transitions at the band edges primarily along *b*-axis ($\varepsilon_{2,yy}(E_g) \gg \varepsilon_{2,xx}(E_g)$), as depicted in Fig. 2(b), and is consistent with previously reported PL behavior.[21] Thus, the pronounced optical anisotropy near the bandgap in CrSBr can be attributed to the dominant contribution of intralayer Cr–S bond along the *b*-axis.

Subsequently, we examined the Raman spectrum of CrSBr. Based on the *Pmnm* (No. 59) space group of CrSBr, we determined that only three Raman-active A_g modes are allowed in the *ab* plane. As shown in Fig. 2(c), these

Raman-active peaks are located at 114 cm^{-1}, 245 cm^{-1}, and 344 cm^{-1}, labeled as A_g^1, A_g^2, and A_g^3, respectively. Although all three modes exhibit two-fold anisotropy in polarization-dependent Raman measurements, the A_g^1 and A_g^3 modes display an anisotropy opposite to that of the A_g^2 mode. This behavior arises from the anisotropic Raman tensor $R(A_g)$ along the *a*- and *b*-axes (Note S5, supplementary material), which influence the polarization state of the Raman spectra.[22,29] To further investigate the phonon vibration modes of the Raman peaks, we calculated the phonon spectrum of CrSBr. The calculated frequencies for the three A_g modes are 121.0 cm^{-1}, 245.0 cm^{-1}, and 346.6 cm^{-1}, respectively, which are in close agreement with our experimental values. Due to symmetry constraints, the phonon vibrations of the three A_g modes are all along the *c*-direction (Note S5, supplementary material). In particular, the highest A_g^3 mode primarily involves the relative vibrations between interlayer Cr and S atoms within each quasi-monolayer, as illustrated in Fig. 2(d). On the other hand, the contribution from Br atoms vibrations is negligible due to their relatively large mass.

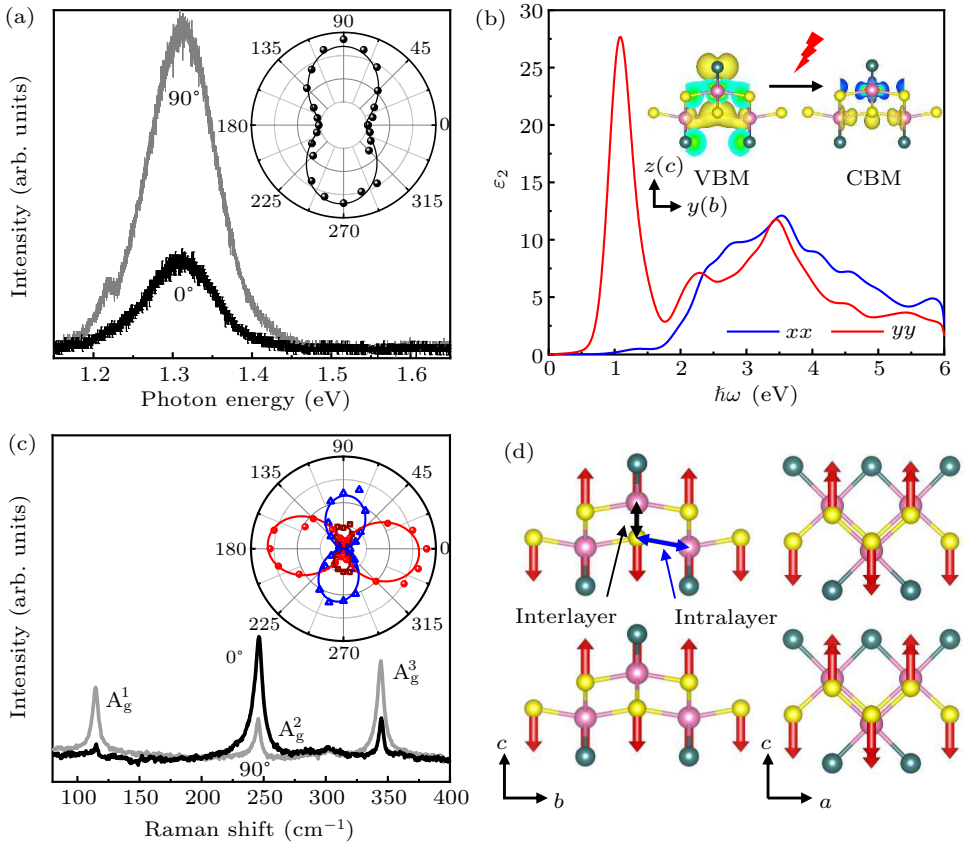


Fig. 2. (a) PL spectra of unstrained CrSBr with linearly polarized light parallel to the *a*-axis (0°) and *b*-axis (90°), respectively. Inset: polarization-dependent PL peaks of CrSBr without strain. (b) The imaginary part of the dielectric function calculated by DFT. Note that the peak positions in the calculated dielectric function are smaller than the PL peaks, which is due to the underestimation of the bandgap by DFT (calculated value is 0.85 eV). Inset: The charge density at the conduction band minimum (CBM) and valence band maximum (VBM). (c) Raman spectra of unstrained CrSBr with linearly polarized light parallel to the *a*-axis (0°) and *b*-axis (90°), respectively. Inset: polarization-dependent Raman peaks. (d) The vibration of the Raman mode A_g^3. The black and blue double-arrows denote the interlayer and intralayer Cr–S bonds in the quasi-monolayer, respectively.

Building on the above elucidation of the roles played by intralayer and interlayer Cr–S bonds of unstrained CrSBr in PL and Raman spectroscopy, we next investigated the effects of strain by applying uniaxial tensile strain simultaneously along both the *a*- and *b*-axes. To achieve this, two perpendicular CrSBr flakes with comparable thickness were assembled into a single flexible film using an encapsulation technique (Fig. 3(a), Note S1, supplementary material), thereby ensuring that identical tensile strain is applied simultaneously along both the *a*- and *b*-axes (Fig. S3, supplementary material). As shown in Figs. 3(b) and 3(c), with increasing tensile strain, the peak positions along both the *a*- and *b*-axes decrease. This trend suggests a reduction of bandgap and a shrink of the energy difference between the bonding state at the VBM and the antibonding state at the CBM. Then, PL peak positions were extracted at various strain and were plotted in Fig. 3(d), which reveals that the bandgap under the *b*-axis strain changes more significantly than that under the *a*-axis strain, with a linear dependence on the applied strain. This observation unambiguously indicates a direction-dependent strain effect on the electronic structure. Notably, a marked decrease in PL peak intensity is observed when strain is applied along the *b*-axis (Fig. 3(c)). This intensity reduction can be attributed to the tensile strain-induced bandgap narrowing, which diminishes

the probability of direct radiative electron–hole recombination transitions, ultimately leading to lower PL intensity.[30–32]

To explain the above experimental findings, we calculated the bandgap of CrSBr as a function of strain using DFT. Although conventional DFT tends to underestimate absolute bandgap values due to the inherent defects of delocalization error and derivative discontinuity,[33] it reliably describes trends in the change of bandgap qualitatively. Our calculations indicate that while tensile strain applied along either crystallographic direction decreases the bandgap, the magnitude of this reduction is significantly greater for strain along the *b*-axis compared to the *a*-axis (Fig. 3(e)). This behavior is primarily attributed to the fact that the wavefunctions of CBM and VBM in CrSBr are predominantly derived from intralayer Cr–S bonds that are aligned along the *b*-axis (the inset of Fig. 2(b)). Consequently, tensile strain along the *b*-axis is expected to substantially elongate these intralayer Cr–S bonds, whereas strain along the *a*-axis exerts a relatively minor influence. To validate this hypothesis, we calculated the changes of the intralayer Cr–S bond lengths under different strain conditions. As depicted in Fig. 3(f), the strain along the *b*-axis significantly increases the Cr–S bond distances, while the strain along the *a*-axis has only a minor effect. Moreover, our calculations suggest that the Poisson's ratio of CrSBr is approximately three times lower than those of other 2D materials (Note S7, supplementary material), which implies the presence of hybrid bonding characteristics in this material.[34,35] In a short conclusion, both our theoretical and experimental results demonstrate that the tensile strain along the *b*-axis can significantly modulate the electronic structure of the CBM and VBM, thereby offering considerable potential for tuning the optical properties of CrSBr.

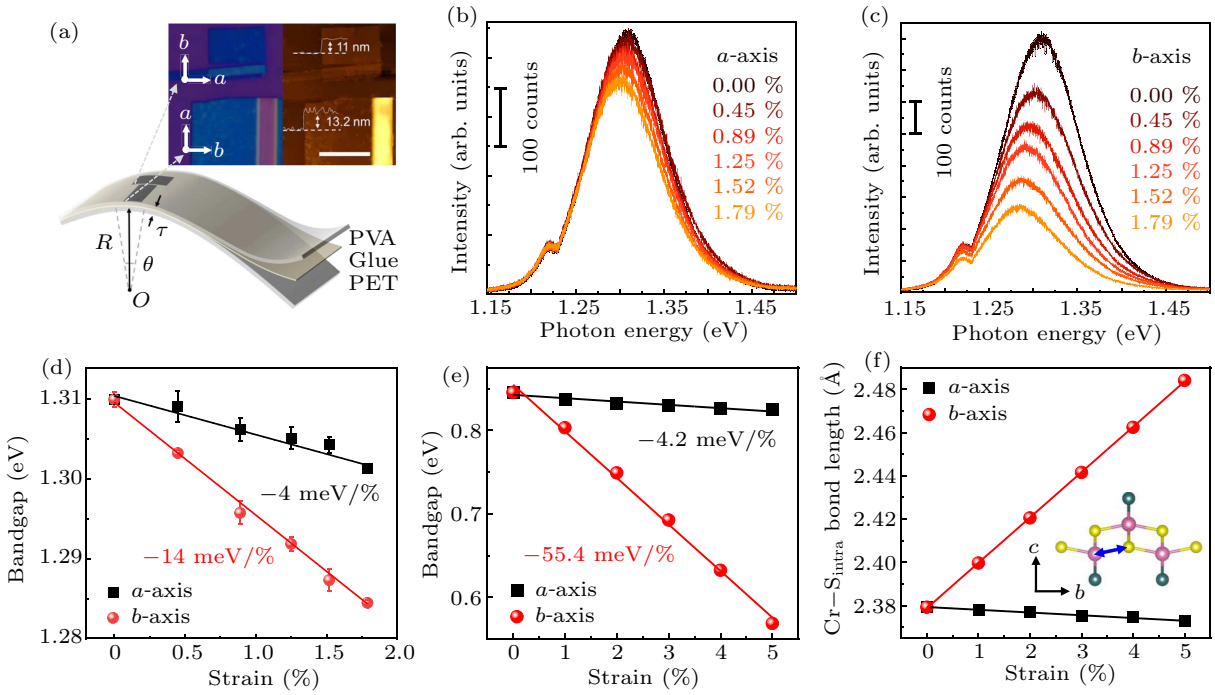


Fig. 3. (a) Schematic diagram for applying uniaxial strain along different directions simultaneously. Inset: Optical photograph and atomic force microscopy (AFM) images of the two perpendicular CrSBr flakes on Si/SiO_2 substrate. The line profiles of the AFM show the thickness of the two CrSBr flakes, indicating the similar thickness. Scale bar is 5 μm. (b)–(c) The PL spectra under the uniaxial strain along *a*-axis and *b*-axis, respectively. (d) The extracted PL peak position from panels (b) and (c) as a function of strain. The black and red lines are the linearly fitting lines along *a*-axis and *b*-axis, respectively. (e) The calculated bandgap with strain and the linear fitting lines. (f) The calculated intralayer Cr–S bond length. Inset: The blue arrow indicates the intralayer Cr–S bond.

To investigate the strain effects on the interlayer Cr–S bonds, we examined the behavior of the Raman spectra under applied strain. As shown in Fig. 4(a), increasing tensile strain induces a redshift in all three Raman peaks, suggesting that the atomic vibrational modes are weakened and that the vibrational frequencies decrease with strain. By extracting the positions of these peaks as functions of strain, we observed that the A_g^3 mode exhibits a more pronounced response than the A_g^1 and A_g^2 modes for strain applied along either the *a*-axis or the *b*-axis (Figs. 4(b) and S4, supplementary material). More importantly, it is observed that the changes of strain response of Raman spectrum are opposite to those of the PL spectrum, with the Raman shifts along the *a*-axis changing more significantly than those along the *b*-axis (Fig. 4(b)). This behavior suggests the different bond responses on these two spectra. To elucidate the mechanism underlying these observations, we performed first-principles calculations of the phonon spectrum of CrSBr under strain. The results reveal that the phonon frequency of the A_g^3 mode decreases under strain along the *a*-axis, whereas it increases slightly with tensile strain along the *b*-axis (Fig. 4(c)), a trend that is qualitatively consistent with the experimental results.

Although the A_g^3 mode primarily involves the relative motion between Cr–S pairs across two sublayers (*i.e.*, the interlayer Cr–S bonds), the effects of strain along the two different directions on the interlayer Cr–S bond distances may not be isotropic, which will lead to different behaviors in the Raman response. Accordingly, we calculated the interlayer Cr–S bond lengths under strain and found that the tensile strain along the *a*-axis increases the bond length, while the strain along the *b*-axis decreases it (Fig. 4(d)). This finding explains the divergent Raman responses observed in experiments under the two strain directions. Moreover, these results provide direct evidence that the tensile strain on the rhombohedral bonds configuration results in the elongation of all bonds (as depicted in Fig. 1(a)), whereas for rectangular bonds configuration, the strain stretches the bonds that are parallel to the strain direction and compresses those that are perpendicular (as illustrated in Fig. 1(b)).

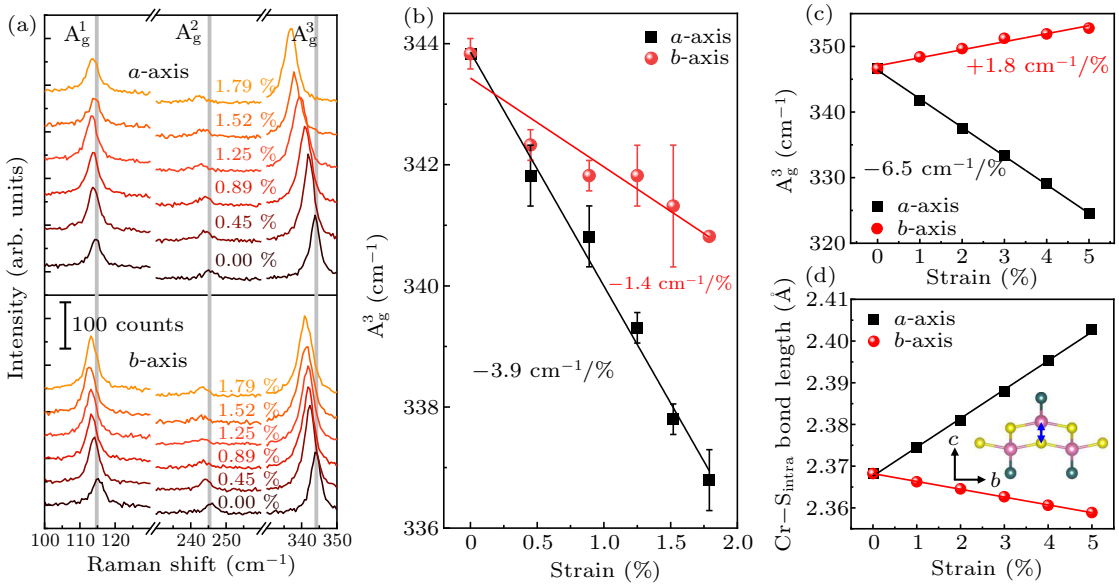


Fig. 4. (a) Strain-induced Raman spectra under applied strain along *a*-axis and *b*-axis, respectively. The gray lines are the guide to show the Raman peak position changes under strains. (b) The peak position of A_g^3 mode with strains. (c) Theoretical calculated A_g^3 frequency with strains. (d) The calculated interlayer Cr–S bond length. Inset: The blue arrow indicates the interlayer Cr–S bond.

In summary, we systematically investigated the photoluminescence and Raman spectra of CrSBr under uniaxial strain, revealing a non-synchronous strain response. Our findings indicate that the PL spectrum is predominantly sensitive to tensile strain applied along the *b*-axis, whereas the Raman spectrum of A_g^3 mode is more responsive to strain along the *a*-axis. This contrasting behavior arises from the distinct responses of the interlayer and intralayer Cr–S bonds to the applied tensile strains. Our work not only deepens the understanding of the fundamental properties of CrSBr but also provides critical insights for the design and optimization of its electronic and optoelectronic devices.

Supplementary material

Supplementary material includes ample preparation, setup for Raman and PL measurement, thickness-dependent Raman and PL spectrums of CrSBr, strain calculation method, symmetry of Raman modes of CrSBr, density functional theory (DFT) calculations, calculation of Passion's ratio of CrSBr, strain dependence of the Raman modes A_g^1 and A_g^2, repeatability for strain application.

Acknowledgements

Project supported by the National Natural Science Foundation of China (Grant Nos. 52471248, 12174364, 12204009, and 12104003), the Natural Science Foundation of Anhui Province, China (Grant No. 2308085Y04), the National Key Research and Development Program of China (Grant No. 2023YFA1406400), and the Fundamental Research Funds for the Central Universities (Grant No. wk2310000104).

References

[1] Park J G 2016 *J. Phys.: Condens. Matter* **28** 301001
[2] Yagmurcukardes M, Bacaksiz C, Unsal E, Akbali B, Senger R T and Sahin H 2018 *Phys. Rev. B* **97** 115427
[3] Du Y, Maassen J, Wu W, Luo Z, Xu X and Ye P D 2016 *Nano Lett.* **16** 6701
[4] Deng Y, Zhang Y, Zhao Y, Xu Y, Dai X, Wang S, Lu X, Li Y, Xu Y and He L 2024 *Chin. Phys. Lett.* **41** 037102
[5] Zhang S, Mao N, Wu J, Tong L, Zhang J and Liu Z 2017 *Small* **13** 1700466
[6] Li L, Han W, Pi L, Niu P, Han J, Wang C, Su B, Li H, Xiong J, Bando Y and Zhai T 2019 *InfoMat* **1** 54
[7] Iqbal M W, Shahzad K, Akbar R and Hussain G 2020 *Microelectron. Eng.* **219** 111152
[8] Li Z, Lv Y, Ren L, Li J, Kong L, Zeng Y, Tao Q, Wu R, Ma H, Zhao B, Wang D, Dang W, Chen K, Liao L, Duan X, Duan X and Liu Y 2020 *Nat. Commun.* **11** 1151
[9] Samal R, Sanyal G, Chakraborty B and Rout C S 2021 *J. Mater. Chem. A* **9** 2560

[10] Yu W, Wang Z, Zhao X, Wang J, Herng T S, Ma T, Zhu Z, Ding J, Eda G, Pennycook S J, Feng Y P and Loh K P 2020 *Adv. Funct. Mater.* **30** 2003057

[11] Zhao Y, Du Z, Wang L, Liu M, Yao B, Hu X, Gao L, Wu F, Liu C, Li X, Wan Y and Kan E 2023 *ACS Appl. Nano Mater.* **6** 9679

[12] Telford E J, Dismukes A H, Dudley R L, Wiscons R A, Lee K, Chica D G, Ziebel M E, Han M G, Yu J, Shabani S, Scheie A, Watanabe K, Taniguchi T, Xiao D, Zhu Y, Pasupathy A N, Nuckolls C, Zhu X, Dean C R and Roy X 2022 *Nat. Mater.* **21** 754

[13] Wang Q H, Bedoya-Pinto A, Blei M, Dismukes A H, Hamo A, Jenkins S, Koperski M, Liu Y, Sun Q C, Telford E J, Kim H H, Augustin M, Vool U, Yin J X, Li L H, Falin A, Dean C R, Casanova F, Evans R F L, Chshiev M, Mishchenko A, Petrovic C, He R, Zhao L, Tsen A W, Gerardot B D, Brotons-Gisbert M, Guguchia Z, Roy X, Tongay S, Wang Z, Hasan M Z, Wrachtrup J, Yacoby A, Fert A, Parkin S, Novoselov K S, Dai P, Balicas L, Santos E J G, *et al.* 2022 *ACS Nano* **16** 6960

[14] Ye C, Wang C, Wu Q, Liu S, Zhou J, Wang G, Söll A, Sofer Z, Yue M, Liu X, Tian M, Xiong Q, Ji W and Renshaw Wang X 2022 *ACS Nano* **16** 11876

[15] Pei F, Yu J, Zhou J, Wang S, Liu D, Yuan Y, Xi L, Jin F, Kan X, Wang C, Wang L, Yan W, Wu Y, Wang S, Chen K, Ma T, Liu X, Yang M and Li Q 2023 *Adv. Funct. Mater.* **34** 2309335

[16] Yu J, Liu D, Ding Z, Yuan Y, Zhou J, Pei F, Pan H, Ma T, Jin F, Wang L, Zhu W, Wang S, Wu Y, Liu X, Hou D, Gao Y, Qiu Z, Yang M and Li Q 2023 *Adv. Funct. Mater.* **34** 2307259

[17] Cenker J, Sivakumar S, Xie K, Miller A, Thijssen P, Liu Z, Dismukes A, Fonseca J, Anderson E, Zhu X, Roy X, Xiao D, Chu J H, Cao T and Xu X 2022 *Nat. Nanotechnol.* **17** 256

[18] Bagani K, Vervelaki A, Jetter D, Devarakonda A, Tschudin M A, Gross B, Chica D G, Broadway D A, Dean C R, Roy X, Maletinsky P and Poggio M 2024 *Nano Lett.* **41** 13068

[19] Lan G, Xu H, Zhang Y, Cheng C, He B, Li J, He C, Wan C, Feng J, Wei H, Zhang J, Han X and Yu G 2023 *Chin. Phys. Lett.* **40** 058501

[20] Wilson N P, Lee K, Cenker J, Xie K, Dismukes A H, Telford E J, Fonseca J, Sivakumar S, Dean C, Cao T, Roy X, Xu X and Zhu X 2021 *Nat. Mater.* **20** 1657

[21] Klein J, Pingault B, Florian M, *et al.* 2023 *ACS Nano* **17** 5316

[22] Panda J, Sahu S, Haider G, Thakur M K, Mosina K, Velický M, Vejpravova J, Sofer Z and Kalbáč M 2023 *ACS Appl. Mater. Interfaces* **16** 1033

[23] Beck J 2004 *Z. Anorg. Allg. Chem.* **585** 157

[24] Yang K, Wang G, Liu L, Lu D and Wu H 2021 *Phys. Rev. B* **104** 144416

[25] Shang C, Wang W, Zhang J, Zhao Y, Li J, Chen L, Jia G, Zhou N, Liu G, Hui M, Huang H, Zhang L, Dong G, Zhang J, Xu H, Li X and Yang R 2024 *Adv. Funct. Mater.* **34** 2410783

[26] Kresse G and Furthmüller J 1996 *Phys. Rev. B* **54** 11169

[27] Kresse G and Joubert D 1999 *Phys. Rev. B* **59** 1758

[28] Linhart W M, Rybak M, Birowska M, Scharoch P, Mosina K, Mazanek V, Kaczorowski D, Sofer Z and Kudrawiec R 2023 *J. Mater. Chem. C* **11** 8423

[29] Torres K, Kuc A, Maschio L, Pham T, Reidy K, Dekanovsky L, Sofer Z, Ross F M and Klein J 2023 *Adv. Funct. Mater.* **33** 2211366

[30] Desai S B, Seol G, Kang J S, Fang H, Battaglia C, Kapadia R, Ager J W, Guo J and Javey A 2014 *Nano Lett.* **14** 4592

[31] Ghosh P, Farooq U, Su H, Pei S, Li G, He W, Dai J, Huang L and Huang M 2022 *J. Mater. Sci.* **57** 5061

[32] Sharma J, Reynolds B, Crane M J and Packard C E 2024 *J. Phys. Chem. Lett.* **15** 4294

[33] Perdew J P and Levy M 1983 *Phys. Rev. Lett.* **51** 1884

[34] Liu N, Wang C, Zhang Y, Pang F, Cheng Z, Zhang Y and Ji W 2024 *Phys. Rev. B* **109** 214422

[35] Deng S, Sumant A V and Berry V 2018 *Nano Today* **22** 14